Attracting retinal cells to electrodes for high-resolution stimulation

Daniel V. Palanker[1,2], Philip Huie[1,2], Alexander Vankov[1,2], Yev Freyvert[2], Harvey Fishman[1], Michael F. Marmor[1], Mark S. Blumenkranz[1]

[1] *Department of Ophthalmology, Stanford University, 300 Pasteur Dr., Stanford, CA 94305-5308;*
[2] *Hansen Experimental Physics Laboratory, Stanford University, Stanford, CA, 94305-4085*

ABSTRACT

Development of the electronic retinal prosthesis for restoration of sight in patients suffering from the degenerative retinal diseases faces many technological challenges. To achieve significant improvement in the low vision patients the visual acuity of 20/80 would be desirable, which corresponds to the pixel size of 20μm in the retinal implant. Stimulating current strongly (quadratically) depends on distance between electrode and cell. To achieve uniformity in stimulation thresholds, to avoid erosion of the electrodes and overheating of tissue, and to reduce the cross-talk between the neighboring pixels the neural cells should not be separated from electrodes by more than a few micrometers. Achieving such a close proximity along the whole surface of an implant is one of the major obstacles for the high resolution retinal implant.

To ensure proximity of cells and electrodes we have developed a technique that prompts migration of retinal cells towards stimulating sites. The device consists of a multilayered membrane with an array of perforations of several (5-15) micrometers in diameter in which addressable electrodes can be embedded. In experiments in-vitro using explants of the whole retina of P7 rats, and in-vivo using adult rabbits and RCS rats the retinal tissue grew into the pores when membranes were positioned on the sub-retinal side. Histology has demonstrated that migrating cells preserve synaptic connections with cells outside the pores, thus allowing for signal transduction into the retina above the implant.

Intimate proximity of cells to electrodes achieved with this technique allows for reduction of the stimulation current to 2μA at the 10μm electrode. A 3mm disk array with 18,000 pixels can stimulate cells with 0.5 ms pulses at 50Hz while maintaining temperature rise at the implant surface below 0.3 ^{o}C. Such an implant can, in principle, provide spatial resolution geometrically corresponding to the visual acuity of 20/80 in a visual field of 10^{o}.

Key words: Retinal prosthesis, neural cell stimulation, visual acuity

1. INTRODUCTION

The first steps are being taken towards use of an electronic retinal implant for restoration of vision in patients that have lost their sight from degenerative retinal diseases. It has been demonstrated that degenerated retina responds to patterned electrical stimulation in a manner consistent with form vision[1, 2]. Recent tests of chronic stimulation in humans using an array of 4x4 electrodes of 0.4mm in size have shown recognition of simple patterns and shapes[3].

A large percentage of patients with age-related macular degeneration (AMD) preserve visual acuity on the level of about 20/400 due to peripheral vision, and implantation would be worth its risk only if it provided substantial improvement in the central field. In contrast, patients with advanced retinitis pigmentosa would benefit from prosthesis with an enlargement of the central visual field to allow reasonable ambulation. Normal visual acuity (20/20) corresponds to angular separation of lines by 1 min[4], which corresponds to spatial separation on the retina of about 10μm. The minimal pixel size required for such resolution is 5 μm. Thus visual acuity at the level of 20/400 corresponds to a pixel size of about 100μm, while acuity of 20/80 (enough for reading with some visual aids) requires pixels less than 20μm. For functional restoration of sight the array should ideally cover at least 10^{o} of the visual field (3 mm on retina), and support a visual acuity of at least 20/80 in the central 2-3^{o}. Since peripheral vision has lower visual acuity, the pixel density could, in principle, decrease radially. However, because surgical localization of a chip may have a degree of uncertainty, and the critical stimulation areas may involve dense arrays of bipolar or ganglion cells in the parafovea, it may be desirable to preserve a high pixel density within much of the disk. It is also important to keep in mind that functional vision will be easier to achieve if the number of stimulating elements is not at the minimum level. An array of 20μm pixels would have a density of 2500 pixels/mm^2, which would amount to 18,000 pixels in a 3mm chip.

Electrical stimulation of neural cells in the retina has been achieved with an array of electrodes positioned on either the inner[1,5,6] or outer side of retina[7-9]. Setting the electrodes into the subretinal space with electrical

stimulation of the bipolar cells, although surgically challenging, has the potential advantage that signal processing in retina is partially preserved, as opposed to the excitation of ganglion cells with electrodes positioned on the epiretinal side. One of the concerns with either technique, with respect to high resolution stimulation, is that the electrodes will always be some distance from the target cells. In epiretinal approach this occurs because the implant is separated by inner limiting membrane and nerve fiber layer. In the case of sub-retinal implantation the photoreceptor remnants or subretinal scar tissue may get in the way. In addition, diseased retina may have uneven thickness and wavy structure, and may not lie flat on the electrode array, leading to further separation of cells from electrodes. Large distances between the cells and electrodes result in cross-talk between neighboring electrodes, and make necessary a high charge density and power for cell stimulation. This, in turn, may lead to erosion of electrodes and excessive heating of the tissue, all of which limit spatial resolution. Furthermore, variability in the distance between electrodes and cells in different parts of the implant will result in strong variations of the stimulation threshold, making it necessary to adjust the signal intensity in each pixel.

2. PHYSICAL LIMITATIONS ON RESOLUTION OF THE STIMULATING ARRAY

For quantitative assessment of various electrochemical and thermal effects limiting resolution of the retinal stimulating array we use a passive model of extracellular stimulation of the cell body [10]. The typical resting potential of a neural cell is in the range of -60-70 mV [11], and depolarization of the cell membrane by 5-25 mV is sufficient for eliciting a physiological response, including the graded potential neurons such as bipolar retinal cells[12, 13]. In order to achieve this level of cross-membrane depolarization with extracellular stimulation, a cross-cellular potential is typically induced by application of an electric field to the surrounding medium. Since the impedance of the cellular membrane (R_{mem} ~5 MOhm-5GOhm [14]) is much higher than that of the cellular cytoplasm (R_{cyto} ~ 100 kOhm), the interior of a cell quickly becomes equipotential so that the trans-membrane potential is increased (hyperpolarized) on the anode side of the cell and similarly decreased (depolarized) on the cathode side[10], as shown in Figure 1. To achieve depolarization of the cell membrane by say 15 mV [10, 15] the cross-cellular voltage should be twice this amount (i.e. ΔU=30 mV).

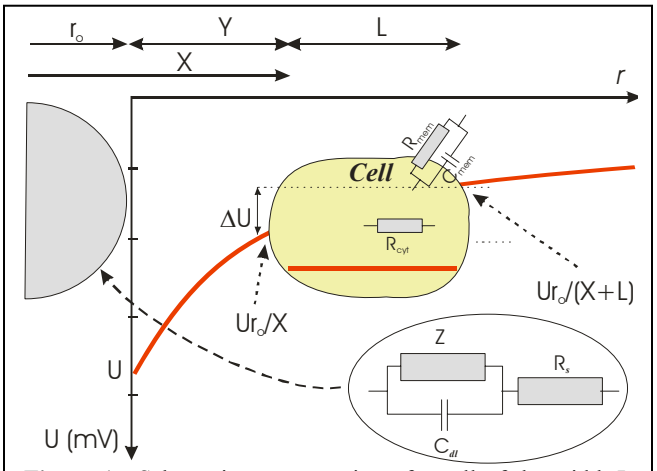

Figure 1. Schematic representation of a cell of the width L positioned on distance X from the center of a hemispherical electrode with radius r_o, (distance Y from its surface). The cross-cell voltage is ΔU. The electrode-liquid interface is shown in the insert. It includes a capacity C_{dl}, faradaic impedance Z, and ohmic resistance of solution R_s.

For a hemispherical electrode of radius r_o embedded into an insulating plane, as shown in Figure 1, with the large return electrode at infinity, the resistance of the conductive medium will be [16, 17]: $R_s = \gamma /(2\pi r_o)$, where γ is the resistivity of the physiological solution (e.g. γ = 70 Ohm·cm for saline). The resistive potential drop in the solution U_s required for generation of the cross-cellular voltage ΔU is:

$$U_s = \Delta U \frac{x(x+L)}{r_0 L} \quad (1)$$

The corresponding current density will be:

$$j_e = \frac{E_e}{\gamma} = \Delta U \frac{x(x+L)}{\gamma r_0^2 L} \quad (2)$$

The total current on electrode:

$$I_e = j_e \cdot 2\pi r_o^2 = \Delta U \frac{2\pi x(x+L)}{\gamma L} \quad (3)$$

The required U_s and I_e are minimal when a cell is touching the electrode, i.e. when $x=r_o$, $U_{s\,min}=\Delta U(r_0+L)/L$; $I_{e\,min}=2\pi\Delta U \cdot r_0(r_0+L)/\gamma L$. The minimal threshold voltage and current both decrease with radius of electrode, however, if it becomes much smaller than the cell, the electric field will be concentrated in a small area in the proximity of the electrode, while the rest of the cell membrane will not be affected. Thus the optimal size of an electrode designed for selective stimulation of a single cell should be comparable to the cellular size ($L \approx 10$ μm), i.e. its radius r_o should be about 5μm.

As follows from the equations 1-3, the threshold voltage and current required for stimulation of a neuron depend strongly on the size of the electrode and on the distance between the electrode and the cell. As shown in Figure 2, the lowest current (2 μA) is required with the smallest electrode size (r_o=5μm) when the 10 μm cell is in contact with its surface, but it increases by an order of magnitude when cell is separated from this electrode by just 25μm. The larger electrodes require higher threshold current, but are more tolerant to changes in the separation distance, i.e. the threshold potential does not rise as rapidly with distance as for smaller electrodes. For example, if we define the "tolerance range" as a distance over which the threshold potential changes by a factor of 2, it is only 3μm for an electrode radius of 5 μm, and 65μm for the electrode radius of 150 μm. If the distance between electrodes and cells varies for different parts of the array, the stimulation threshold (and the visual outcome) will vary accordingly. **Close and stable proximity of cells to the electrodes is thus a very important issue in the design of a high-resolution retinal implant.**

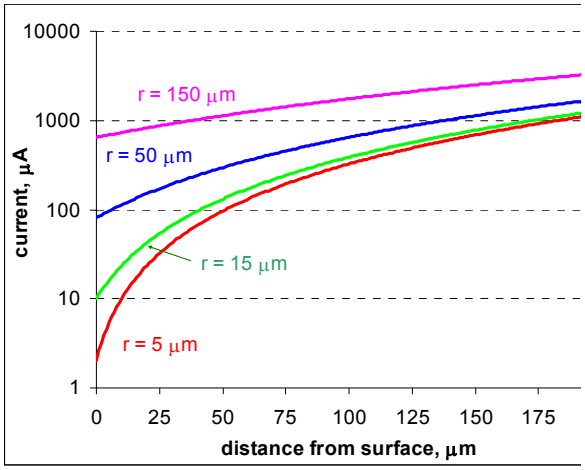

Figure 2. Threshold current required to generate a 30 mV voltage drop across a 10 μm–long cell, plotted as a function of distance between the cell and the electrode surface. Calculated for electrode radii of 5, 15, 50 and 150 μm.

Cross-talk between electrodes

One of the reason for degradation of resolution when cells are separated from the stimulus electrodes is cross-talk between neighboring stimulus pixels, i.e. the stimulation of one cell by a few neighboring electrodes. Assuming that the dynamic range of prosthetic stimulation should be similar to the range of depolarization voltage under natural conditions, which is greater than 10 dB [12, 13], the interference from the neighboring electrode should be less than $1/10^{th}$ of the local electric field. Thus, for a cell located at distance *X* from the primary electrode, as in Figure 3, the electric field from a neighboring electrode will be 10 times lower if separation between the centers of the electrodes is 3*X* (electric field $E \propto 1/R^2$, and $R^2=x^2+(3x)^2=10x^2$). This minimal distance (3*x*) between pixels determines the maximal pixel density $n = 1/(3x)^2$ which limits the number of pixels on an array. Figure 4 shows the maximal pixel density as a function of distance between electrodes and cells determined by the cross-talk. Horizontal dashed lines indicate pixel densities corresponding (geometrically) to various levels of visual acuity. For example, to operate 2,500 pixels/mm^2 (visual acuity 20/80) the separation of cells from electrodes (*Y*) should not exceed 7μm. If the cells are 50μm away, cross-talk would limit the density to only 44 pixels/mm^2.

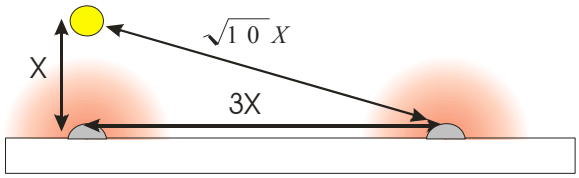

Figure 3. Diagram of the electric fields produced by two neighboring electrodes, and affecting a cell located at distance X in front of one of them.

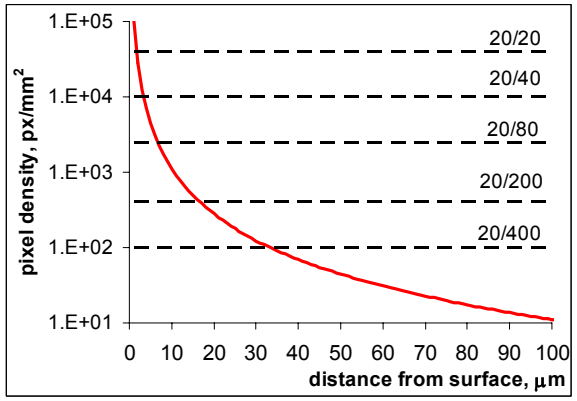

Figure 4. The cross-talk limit on the pixel density as a function of distance between electrodes and cells. Interference level from the neighboring pixels is set to 10% of the primary electric field. Horizontal dashed lines indicate pixel densities corresponding (geometrically) to various levels of visual acuity.

Electrochemical limitation

Current across an electrode/electrolyte interface can be produced by two mechanisms: (i) charging/discharging of the electrical double layer, known as capacitive coupling, and/or (ii) electron transfer due to electrochemical reactions at the electrode surface, known as faradaic process. The equivalent scheme of the interface between electrode and

electrolyte, illustrating these two paths is shown in the insert in Figure 1. Typically the capacitance of the double layer on metal electrodes is much lower than what is needed for cellular stimulation [18]. Metal electrodes, as have been used to date in prosthetic implants, involve faradaic coupling which allows higher charge density to be transferred through the electrode-electrolyte interface. However, above certain limits the generation of gas and erosion of the electrode material will occur. The maximal "safe" charge densities on Pt, AgCl and IrOx electrodes allowing the gas-free and erosion-free operation are 0.4 mC/cm^2 [19], 2.5 [18] and 4 mC/cm^2 [20, 21], respectively. The maximal charge density determines the minimal size of the electrode required for "safe" operation as a function of distance between electrodes and cells. Assuming that the neighboring electrodes in the array are separated by the 3 radii of the electrode (the cross-talk limit), the maximal pixel density can be calculated as following: $n=1/(9r_o^2)$. This maximal pixel density is calculated for pulse duration of 0.5 ms and plotted in Figure 5 as a function of distance between electrode and cell for the Pt, AgCl and IrOx electrodes. For comparison, we plot on the same graph the pixel densities geometrically corresponding to various levels of visual acuity (horizontal dashed lines). As one can see in this plot, the electrodes made of Platinum are limited in the pixel density to about 500 pix/mm^2 (corresponding to visual acuity of about 20/200), even if cells are in direct contact with electrodes. This number drops to only 17 pix/mm^2 when cells are separated from the electrodes by 25 μm. Pixel density of 2,500 pix/mm^2 (corresponding to visual acuity 20/80) can be achieved at distances up to 6 μm and 17 μm using the AgCl and IrOx electrodes, respectively.

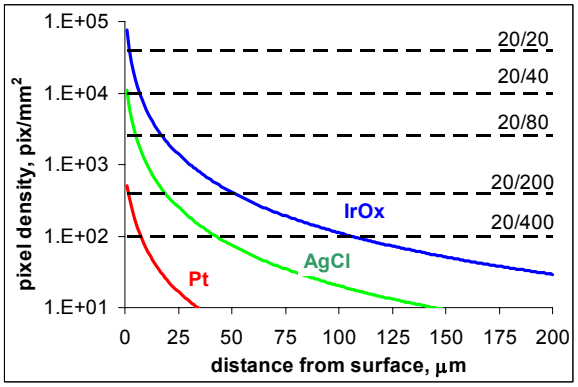

Figure 5. Maximal pixel density as a function of the distance between electrodes and cells. Limits are imposed by maximal charge density on Pt, AgCl and IrOx electrodes.

Tissue heating

Electrical current in a conductive medium and at the metal/liquid interface generates Joule heat. Heating limits the number of pixels per unit area of an implant because of potential hyperthermia of tissue. With a continuous train of pulses the heat diffusion into the surrounding liquid creates a steady distribution of temperature. Power dissipation from a disk-shaped implant of diameter D surrounded by liquid with thermal conductivity λ having the ambient temperature at infinity is[22]: $P_{heat} = 4\,\lambda\cdot\Delta T\cdot D$. Assuming the size of an electrode array being D=3mm, λ being a thermal conductivity of water (0.58W/m·K), and maximal temperature elevation at the implant surface $\Delta T = 1^oC$, results in $P_{heat} \approx 7$ mW. This limit on power dissipation by the implant translates into a limitation on the number of electrodes as a function of distance between them and the cells. As shown in Figure 6 for IrOx electrodes array of 3 mm in diameter, when the cells are in close proximity to electrodes, the maximal pixel density is limited by packing density rather than by heating. Maximal packing density is estimated assuming the minimal separation between electrodes being equal to radius of the electrode. With electrodes of 5 μm in radius the heating will limit the pixel density at distances larger than 4 μm, and it will be reduced below the level of 2,500 (corresponding to visual acuity of 20/80) at 7μm. If cells are separated from the electrodes by 50 μm the maximal pixel density drops below the level corresponding to visual acuity 20/400.

All three physical factors - cross-talk, electrochemistry and heating limit pixel density as a function of distance from the target cells. For example, to achieve pixel density 2,500 pix/mm^2, corresponding to the visual acuity of 20/80, electrodes should be within about 7 μm from the target cells.

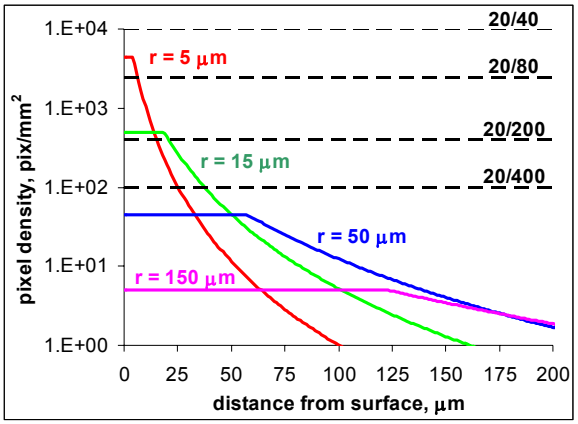

Figure 6. Maximal pixel density in a 3mm implant to keep heating below 1 ^oC at its surface. Calculated for 1 ms pulses applied at rep. rate of 50Hz. via IrOx electrodes. The horizontal segments on each curve represent the packing density limit, corresponding to the electrodes separation (edge-to-edge) by one radius.

3. ATTRACTING RETINAL CELLS TO ELECTRODES

Methods

Mylar membrane, 13 μm in thickness, was perforated on an inverted microscope using tightly focused beam of a picosecond Ti-Sapphire laser. Aperture sizes were varying in the range of 3 to 40 μm. The surface of the membrane was treated with 0.1 mg/ml poly-l-lysine and 0.4 mg/ml laminin diluted in Neurobasal Medium. The perforated membranes were affixed atop polystyrene rings mounted at the center of Petri dishes to form an inner and a surrounding outer chamber. The inner and outer chambers were filled with the same culture media. Some membranes were constructed with an additional basal membrane on one side with 3μm perforations to close the larger pores to cellular passage.

Retinas were harvested from P7 Sprague-Dawley rats (6 samples), 3 week chicken embryos (4 samples), and adult New Zealand White rabbits (3 samples) and positioned onto perforated Mylar membranes. Retinas were incubated for 72 hours in growth media that consisted of Neurobasal Media, pen/strep, insulin, L-glutamine, Sato, and B27. Tuft growth through the perforations was visually monitored with a Nikon TS100 inverted microscope and then processed for histological examination.

For in-vivo experiments, ARVO regulations regarding the use of animals in medical research were followed. Three adult New Zealand White rabbits were anesthetized by intramuscular injection of ketamine (35 mg/kg, Ketaset, Wyeth, Madison, NJ) and xylazine (5 mg/kg, Xyla-Ject, Phoenix Pharmaceutical, Inc., St. Joseph, MO), and a standard 3-port pars planar vitrectomy was performed. A bleb approximately 2 mm in diameter was formed by subretinal injection of BSS with a 40 gauge needle. A retinotomy approximately 1 mm wide was created at the edge of the bleb, and a perforated membrane, 1x2 mm in size, was inserted into the subretinal space through the retinotomy. The retina was flattened with perfluorocarbon, followed by a silicone oil exchange and suturing of the sclerotomy. The eyes were enucleated 3 days after surgery. Two types of membranes were used in these experiments: the 13 μm-thick Mylar film, and a 60 μm-thick regenerated cellulose dialysis membrane with a 15kD pores.

Five albino Royal College of Surgeons (RCS) rats received implants at the age of 65 days. The implantation procedure have been described in detail elsewhere [23]. In anesthetized rats (Ketamine 37.5 mg/kg; Xylazine 5 mg/kg), a small incision (~1 mm) was cut trans-sclerally behind the pars plana of the host eye, and the perforated Mylar film (0.8x1.5 mm in size) was placed into the subretinal space, in the back of the eye near the optic disc in the nasal or superior nasal quadrant of the host, using a custom-made implantation tool. Placement of the transplants was evaluated after each surgery by fundus examination. Rats were sacrificed at 5, 7 and 9 days after surgery.

Enucleated eyes were immersion-fixed in 2.5 % glutaraldehyde/2.0 % paraformaldehyde in 0.1 M sodium cacodylate buffer, pH 7.4 or in 0.1 M sodium phosphate buffer, pH 7.2. The cornea was removed 20–50 min. later, and the eyes were postfixed overnight at 4°C. The tissue was washed in 0.1 M sodium cacodylate or 0.1 M sodium phosphate, osmicated in 2% osmium tetroxide, dehydrated in a series of ethanols and washed in anhydrous propylene oxide. The tissues were embedded in either EMbed 812 or LX-112. One micron sections for light microscopy were stained with toluidine blue, while the 100 nm sections for transmission electron microscopy were stained with uranyl acetate and lead citrate.

Results and Discussion

In experiments *in-vitro*, in which retina was placed photoreceptor-side down upon the membrane, a robust migration of retinal tissue was observed in all samples of the rat, chicken and rabbit retina. Results obtained with the P7 rat retina are shown in Figures 7-8. Migration of the outer nuclear layer, outer plexiform layer and inner nuclear layer occurred in all samples with the aperture sizes above 5 μm. The cellular invasion of the aperture appeared to include both glial and neural cellular elements. The tissue migration rate increased with the size of the aperture. A transmission electron micrograph of a section through an aperture (similar to the line A-B, in Figure 7) is shown in Figure 8, and demonstrates the presence of neuronal processes (axons or dendrites) and synaptic structures connecting the migrating cells. These findings indicate the possibility of signal transmission from the stimulated cells to the rest of the retina.

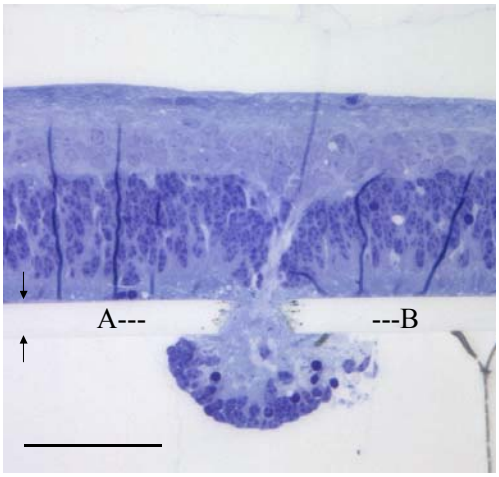

Figure 7. Histological section of the P7 rat retina migrating through a 16 μm aperture in the Mylar membrane. Sample was fixed 72 hours after the explantation. Scale bar is 50 μm.

Culturing of the retina upside down (tested on the P7 rat retina), i.e. nerve fiber layer towards the membrane, did not result in cellular migration.

The RCS rat was chosen as a model for *in vivo* experiments, since the photoreceptors degenerate as in RP. Experiments with subretinal Mylar films perforated with apertures of 15 - 40 μm in diameter showed robust migration of the inner nuclear layer after 5 and 9 days (Figure 9).

In rabbit experiments retinal cells from all layers migrated rapidly through the apertures and around the sides of the implant, leaving almost no tissue above the membrane (results not shown). This occurred most likely because the rabbit retina is avascular and the non-permeable Mylar implant between retina and choriocapillaris made the retina hypoxic except over the apertures. This hypothesis was supported by the observation that rabbit retina remained well-preserved above implants made of a permeable dialysis membrane.

Effect of cellular migration towards a sub-retinal implant can be utilized for bringing the neural cells into proximity of the stimulating electrodes. Two designs of the sub-retinal implants utilizing this effect are shown in Figure 10. The first one, shown in Figure 10A is based on effect of perforated membrane described above. Since unlimited tissue migration through the membrane could be problematic (draining retinal cells and proliferating under the prosthesis) a membrane with pore sizes bellow cellular dimensions can be positioned as a basal seal to prevent growth out the bottom. The addressable electrodes (1) are positioned inside the chambers while the common return electrode (2) is deposited at the top. These experiments were performed in-vitro with cultured rat retinas. After 3-6 days of incubation retinal cells migrated through the 15 μm perforations in the upper membrane into the small inner chambers, while the bottom was sealed with a membrane having tiny (3μm) perforations that would pass nutrients but not cells (results not shown).

Another approach utilizing effect of migration is shown in Figure 10B. In this case the implant has an array of thin electrodes (1) insulated at their sides and exposed at the tops, which protrude above the surface. When positioned under the retina, the cells will migrate into the empty spaces between the electrodes thus assuring penetration of the electrodes into the retina without any pressure and associated risks of mechanical injury. The depth of penetration will be determined by the length of the electrodes. The common return electrode (2) is deposited at the surface of an implant.

The two approaches are complimentary: in the first case the actively migrating cells will penetrate into the pores and will be stimulated. In the second case the migrating cells move towards the bottom of the implant and the electrodes penetrate into the retina approaching the cells which remained in place.

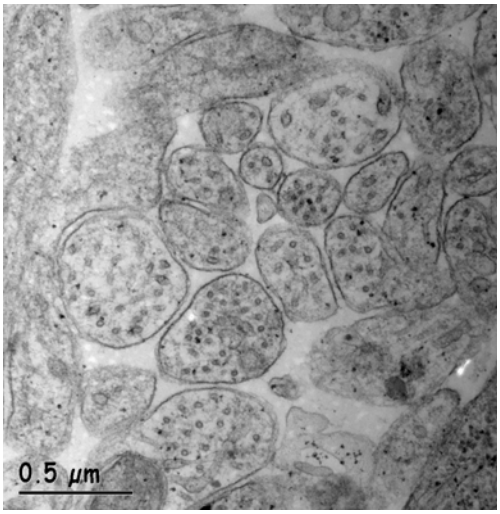

Figure 8. TEM: Cross-section of nerve axons or dendrite within a channel connecting cells within the retina to a migrating tuft. Scale bar is 0.5 μm.

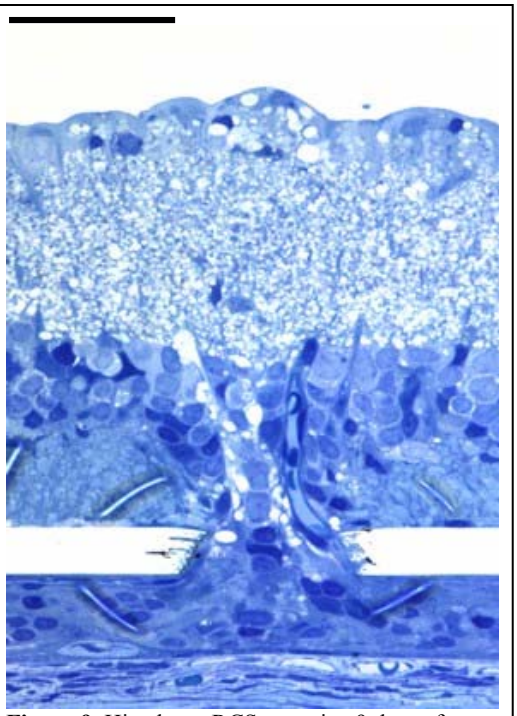

Figure 9. Histology: RCS rat retina 9 days after implantation. Retinal tissue migrates through the aperture of 40 μm and spreads between the RPE and the membrane. Scale bar 50 μm.

The remodeling and potential plasticity of adult retina after injury or degeneration of the photoreceptors has been documented by several investigators [24-29]. There is not only neuronal proliferation but also a growth of non-neural cells including Muller cells and blood vessels[24-29]. After reattachment, Muller cell processes and displaced photoreceptor nuclei can move into the sub-retinal space and spread laterally[25, 26]. The cell processes of displaced Muller cells can form scaffolds that aid in the migration of other retinal neural cells[27], and these may be facilitating the neural retinal migration in our case. Another mechanism of retinal migration involves permeation of the RPE cell extensions deep into the neural retina, and the attraction of small blood vessels from the ganglion cell layer [28]. However RPE cannot be responsible for the retinal migration we observed in-vitro since no RPE was present in that case. The participation of the RPE cells in-vivo will also be prevented if a membrane seals the bottom of an implant, as shown in Figure 10A.

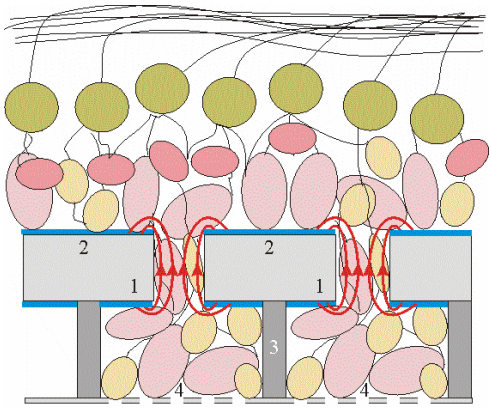

Figure 10A. Cross-sectional diagram of the sub-retinal electrical stimulating array and retina. Biphasic pulses are applied to the inner electrodes in the pores (1). The return electrode (2) is transparent and common to all pixels.

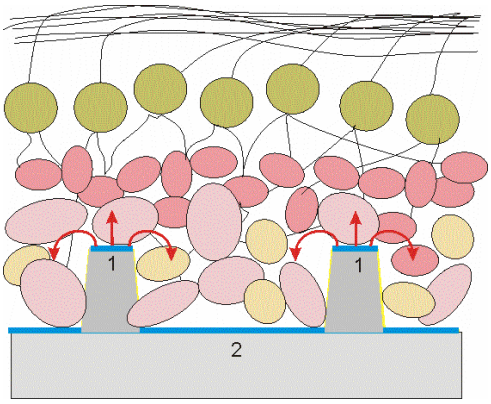

Figure 10B. Design of the sub-retinal implant with protruding electrodes. Retinal cells migrate into the empty spaces between the pillars thus assuring penetration of the electrodes into the inner nuclear layer.

Major concerns are whether the neural cells that migrate into the pores will survive for an extended period of time, and whether the migrated tissue will change through glial overgrowth or cell death. Studies with non-porous sub-retinal implants suggest that the Muller cells can migrate and proliferate, making fibrous tissue and changing neuronal configurations [29, 30]. Proliferation of the glial cells has also been observed with porous membranes implanted on the epiretinal side[31]. The long-term behavior of retinal cells migrating into perforated membranes and between the protruding electrodes should be studied to optimize the implant structure for preserving neural connections and assuring efficacy of an electric interface. Our purpose here is to alert readers to this intriguing phenomenon of neural ingrowth, and to emphasize its potential relevance to prosthetic chip development.

4. CONCLUSIONS

Electrode spacing and potential visual resolution are limited critically by the distance between the electrodes and cells due to potential heating, electrochemical erosion and cross-talk between neighboring pixels. To achieve acuity of 20/200 cell-to-electrode proximity will need to be below 15-20 μm. For acuity of 20/80 that will provide significant improvement to low vision patients, this distance should not exceed 7 μm.

Retinal cells where observed to rapidly migrate into the pores in the sub-retinal implant while preserving their synaptic connections with the retina above. Migration of retinal neurons can be utilized for gaining close proximity between electrodes and target cells to subserve higher resolution. The penetration of cells may also help for mechanical anchoring of a device to tissue. Further studies are needed to explore the long-term stability of the migrated tissue.

Acknowledgements

Authors would like to thank Dr. Robert Aramant and Dr. Magdalene Seiler from Doheney Eye Institute, USCA for help with RCS rat surgery, Kalayaan V. Bilbao and Dimitri Yellachich for help with the rabbit surgery, Thomas Guillaume and Gary Chern for help with membrane fabrication and Roopa Dalal for histological preparations.

Funding is provided in part by the Stanford University Bio-X grant and by the VISX Inc.

REFERENCES

1. Humayun, M.S.,et al, *Pattern electrical stimulation of the human retina.* Vision Research, 1999. **39**(15): 2569-2576.

2. Jensen, R.J., et al., *Thresholds for activation of rabbit retinal ganglion cells with an ultrafine, extracellular microelectrode.* Investigative Ophthalmology & Visual Science, 2003. **44**(8): p. 3533-43.
3. Humayun, M.S. *Clinical Trial Results with a 16-Electrode Epiretinal Implant in End-Stage RP Patients*. in *The First DOE International Symposium on Artificial Sight*. 2003. Fort Lauderdale, FL: Department of Energy.
4. Smith, G. and D.A. Atchison, *The Eye*, in *The Eye and Visual Optical Instruments*. 1997, Cambridge University Press: Cambridge. p. 291-316.
5. Margalit, E., et al., *Visual and electrical evoked response recorded from subdural electrodes implanted above the visual cortex in normal dogs under two methods of anesthesia.* J. Neuroscience Methods, 2003. **123**(2): p. 129-137.
6. Margalit, E., et al., *Retinal prosthesis for the blind.* Survey of Ophthalmology, 2002. **47**(4): p. 335-356.
7. Zrenner, E., et al., *Subretinal microphotodiode arrays to replace degenerated photoreceptors?* Ophthalmologe, 2001. **98**(4): p. 357-363.
8. Stett, A.,et al, *Electrical multisite stimulation of isolated chicken retina.* Vision Research, 2000. **40**(13): 1785-1795.
9. Sachs, H.G., et al., *Subretinal implantation of electrodes for acute in vivo stimulation of the retina to evoke cortical responses in minipig.* Investigative Ophthalmology & Visual Science, 2000. **41**(4): p. S102-S102.
10. Coburn, B., *Neural Modeling in Electrical-Stimulation.* Critical Reviews in Biomed. Eng., 1989. **17**(2): 133-178.
11. Levitan, I.B. and L.K. Kaczmarek, *The Neuron: Cell and Molecular Biology*. 1997, New York: Oxford Univ. Press.
12. Yang, X.L. and S.M. Wu, *Response sensitivity and voltage gain of the rod and cone bipolar cell synapses in dark-adapted tiger salamander retina.* Journal of Neurophysiology, 1997. **78**(5): p. 2662-2673.
13. Berntson, A. and W.R. Taylor, *Response characteristics and receptive field widths of on-bipolar cells in the mouse retina.* Journal of Physiology-London, 2000. **524**(3): p. 879-889.
14. Malmivuo, J. and R. Plonsey, *Hodgkin-Huxley Membrane Model*, in *Bioelectromagnetism*. 1995, Oxford University Press: New York. p. 74-93.
15. Greenberg, R.J., et al., *A computational model of electrical stimulation of the retinal ganglion cell.* Ieee Transactions on Biomedical Engineering, 1999. **46**(5): p. 505-514.
16. Newman, J.S., *Electrochemical systems*. 1973, Englewood Cliffs, NJ: Prentice-Hall.
17. Scharifker, B.R., *Microelectrode Techniques in Electrochemistry*, in *Modern Aspects of Electrochemistry*, J. Bockris, Editor. 1992, Plenum Press: New York. p. 472.
18. Palanker, D., et al., *Physical Constraints on the Design of a High-Resolution Electronic Retinal Prosthesis.* Invest Ophthalmol Vis Sci, 2003. **submitted**.
19. Hesse, L., et al., *Implantation of retina stimulation electrodes and recording of electrical stimulation responses in the visual cortex of the cat.* Graefes Archive for Clinical and Experimental Ophthalmology, 2000. **238**(10): 840-845.
20. Weiland, J.D., D.J. Anderson, and M.S. Humayun, *In vitro electrical properties for iridium oxide versus titanium nitride stimulating electrodes.* Ieee Transactions on Biomedical Engineering, 2002. **49**(12): p. 1574-1579.
21. Meyer, R.D., et al., *Electrodeposited iridium oxide for neural stimulation and recording electrodes.* IEEE Transactions on Neural Systems and Rehabilitation Engineering, 2001. **9**(1): p. 2-11.
22. Rohsenow, W.M., J.P. Hartnett, and E.N. Gani, *Chapter 4*, in *Handbook of heat transfer fundamentals*. 1985, McGraw-Hill. p. 164.
23. Aramant, R.B. and M.J. Seiler, *Retinal transplantation--advantages of intact fetal sheets.* Prog Retin Eye Res, 2002. **21**(1): p. 57-73.
24. Fisher, S.K., et al., *Intraretinal proliferation induced by retinal detachment.* Invest Ophth Vis Sci, 1991. **32**(6): 1739
25. Erickson, P.A., et al., *Retinal detachment in the cat: the outer nuclear and outer plexiform layers.* Invest Ophthalmol Vis Sci, 1983. **24**(7): p. 927-42.
26. Anderson, D.H., et al., *Morphological recovery in the reattached retina.* Invest Ophthalmol Vis Sci, 1986. **27**(2): p. 168-83.
27. Sullivan, R., P. Penfold, and D.V. Pow, *Neuronal migration and glial remodeling in degenerating retinas of aged rats and in nonneovascular AMD.* Investigative Ophthalmology & Visual Science, 2003. **44**(2): p. 856-65.
28. Villegas-Perez, M.P., et al., *Ganglion cell loss in RCS rat retina: a result of compression of axons by contracting intraretinal vessels linked to the pigment epithelium.* J Comp Neurol, 1998. **392**(1): p. 58-77.
29. Marc, R.E., et al., *Neural remodeling in retinal degeneration.* Prog Retin Eye Res, 2003. **22**(5): p. 607-55.
30. Pardue, M.T., et al., *Immunohistochemical studies of the retina following long-term implantation with subretinal microphotodiode arrays.* Exp Eye Res, 2001. **73**(3): p. 333-43.
31. Laube, T., et al., *Biochemical fixation: A new type of epi-retinal implant fixation.* Investigative Ophthalmology and Visual Science, 2000. **41**(4, suppl.S): p. S102-S102.